Fuzzy neural network PID control design of camellia fruit vibration picking manipulator

Ziyan Fan, Lijun Li, Zicheng Gao

College of Mechanical and Electrical Engineering, Central South University of Forestry and Technology, Changsha, China

Abstract

Due to the growth characteristics of the flowers and fruits of camellia in the same period, the vibrating camellia fruit picking machine needs to ensure the constant rotational speed of the vibrating hydraulic motor when the picking mechanism is operating, to achieve a constant vibration frequency, to ensure that the camellia fruit can smoothly fall off the branches through vibration. In contrast, the camellia fruit does not fall off. In this regard, this paper deduced the state space equation of the camellia fruit picking machine's valve-controlled vibrating hydraulic motor system and designed a fuzzy wavelet neural network PID controller (FWNN PID controller) based on the traditional incremental PID control principle. Then the designed vibration picking manipulator control system was simulated under no-load, 5 s load conditions, and load start conditions with MATLAB/Simulink, a general PID controller and a fuzzy RBF neural network PID controller (FRBFNN PID controller) were used to contrast with it. The results show that the general PID controller has a slow response speed and poor robustness, while fuzzy neural network PID controllers (including FWNN PID controller and FRBFNN PID controller) have a fast response speed and strong robustness, which can well meet the requirements of a specific vibration frequency. Finally, a field test was carried out. The results show that the FWNN PID control is better than the FRBFNN PID control. Furthermore, the FWNN PID controller obviously reduced the drop rate of camellia flowers within 6% while ensuring the picking efficiency above 90%, which can well meet the needs of the camellia fruit picking operation.

Correspondence: Li Lijun, College of Mechanical and Electrical Engineering, Central South University of Forestry and Technology, Changsha 410000, China. E-mail: junlili1122@163.com

Key words: camellia fruit picking machine, vibration frequency PID control, fuzzy wavelet neural network.

Acknowledgements: this project was supported by the Key Research and Development Program of Hunan Province of China under Grant 2021NK2023 and the Postgraduate Science and Technology Innovation Fund Project of Central South University of Forestry and Technology (CX202102038).

Conflict of interest: the authors declare no potential conflict of interest.

Received: 21 June 2022.
Accepted: 4 November 2022.

Licensee PAGEPress, Italy
Journal of Agricultural Engineering 2023; LIV:1466
doi:10.4081/jae.2023.1466

Introduction

Camellia is an important oil crop in China, which has high edible and medicinal value (Wang *et al*., 2007). Studies have shown that using camellia to make food can effectively lower blood pressure and prevent cardiovascular and cerebrovascular diseases. In addition, camellia is also widely used to make high-end cosmetics. According to the statistics of the State Forestry and Grassland Administration of China, the planting area of camellia in China reached 45.34 billion square metres in 2020, with a total output value of $17.97 billion, which has driven nearly 2 million people in rural areas to lift themselves out of poverty. However, manual picking is the current primary picking method for camellia fruit. This is because the camellia has the characteristics of the growth of flowers and fruits in the same period. When picking the camellia fruit, it is necessary to avoid the fall of the camellia flowers in order to avoid affecting camellia production in the second year. With the development of China's economy, the labour cost is getting higher and higher, the labour intensity is high, and the picking efficiency is low, severely restricting the development of the camellia industry. Therefore, it is of great significance to realise the mechanised picking of camellia fruit for the development of China's camellia industry.

Currently, the research on mechanised picking of camellia fruit is in its infancy. The basic research directions are mainly divided into comb picking (Gao *et al*., 2013), vibration picking, rubber roller picking (Huang and Rao, 2019), and clamp picking (Zhang *et al*., 2017). Among them, vibration picking has become the current mainstream mechanised picking operation due to its high picking efficiency. The vibrating camellia fruit picking machine mainly relies on the hydraulic motor to drive the vibration-generating mechanism to generate vibration (Gao *et al*., 2019). Due to the different binding force between the camellia flower and camellia fruit and the branch, keeping the rotational speed of the hydraulic motor within a specific range during the picking process can ensure the constant vibration frequency so that the camellia fruit can fall off the branch smoothly while the flowers do not fall off. Therefore, controlling the rotational speed of the hydraulic motor is the key to the design of the vibrating camellia fruit picking machine. At present, the classic control method in the control field is to use the PID controller to carry out closed-loop control of the speed control system, that is, to realise the control of the system by adjusting the three links of propor-

tional, differential, and integral (Karaboga and Akay, 2010; Meng *et al*., 2016; Ayten, 2019; Ayas and Altas, 2018; Yan, 2020). However, the traditional PID controller cannot achieve an ideal control effect for such a complex valve-controlled hydraulic motor system. According to the opinions of references (Lin *et al*., 2019; Wang and Huang, 2019; Kong and Yuan, 2020), fuzzy control does not require precise mathematical models of the controlled object and has strong robustness (Tufan and Serhat, 2022; Han *et al*., 2022; Xu *et al*., 2022). According to the research results from Xue and Fan (2022) and Wu *et al*. (2022), fuzzy PID control has been widely used in robot control in complex environments. Its control effect on PID controllers depends on the richness of experts' experience in this area because fuzzy control needs to rely on expert experience to compile control rules, which becomes a disadvantage of fuzzy PID controllers. Lou and the other researchers (2012) took the lead in introducing fuzzy neural network PID control into the field of fluid control in 2012 and designed a gate flow control system. This controller has advantages of PID controller and fuzzy neural network self-learning and processing quantitative data (Zhou and Chen, 2013) and has better control accuracy and effect. Gong and Yang (2019) began to introduce fuzzy neural network PID control into the field of hydraulic control and designed an oil pump control system suitable for outdoor operations in complex mountainous areas. The controller proved to have good anti-interference ability and good adaptability. However, the electromechanical-hydraulic integrated robots in agriculture and forestry mainly use the hydraulic valve control system for their operation control, and the flow control system of the variable pump is less used due to its high cost. Therefore, this paper uses the fuzzy neural network to control the flow of the valve-controlled hydraulic motor system.

First, this paper analysed the vibrating hydraulic system of a camellia fruit picking machine, clarified the working principle, and established a mathematical model of the system. Then a fuzzy wavelet neural network PID controller (FWNN PID controller) was designed combined with the basic principles of PID control, fuzzy control, and wavelet neural networks. Finally, MATLAB/Simulink was used to simulate and analyse the control system under different working conditions, and field tests were carried out to verify the effectiveness of the control method.

Introduction of control principle and mathematical model

Working principle of camellia fruit picking machine

Introduction of camellia fruit vibration picking manipulator

The push-shake camellia fruit picking machine is a forest fruit vibration picking robot designed by our research group to realise the automatic picking of camellia fruit. This robot integrates mechanics, electronics, and hydraulics, which is different from the mechatronic robots (Wang *et al*., 2015; Gao *et al*., 2016; Wang and Li, 2019; Zhang and Li, 2019) designed by our research team before. As a result, it has a smaller size and structure, lower energy consumption, and more reliable work in the forest working environment. At the same time, the experimental results (Gao *et al*., 2019) show that using a hydraulic system greatly improves the reliability of vibration picking.

The camellia fruit vibration-picking manipulator is the most critical end effector of the push-shake camellia fruit picking machine. Its basic structure is shown in Figure 1. The basic principle of its work is to realise the opening and closing of the gripper through the movement of a bevel gear pair and a ball screw in the clamping mechanism 6 driven by the hydraulic clamping motor 1. Then, the crank link mechanism in vibration mechanism 5 is driven by the vibrating hydraulic motor 1 to generate a push and shake movement to make the camellia fruit branches vibrate. When the exciting force is greater than the binding force between the camellia fruit and the branch, the fruit naturally falls off the branch to realise its mechanised picking.

The quality of control of the vibration frequency output by the vibration mechanism during the picking process will directly affect camellia fruit's quality and picking efficiency since camellia has the characteristics of the same period of flower and fruit growth.

The principle of the hydraulic system of the camellia fruit vibration picking manipulator

The hydraulic system of the camellia fruit vibration-picking manipulator is displayed in Figure 2. A dual-pump oil supply system is designed to meet their respective flow requirements since the hydraulic oil flow required by the picking manipulator to perform positioning and clamping is small, while the hydraulic oil flow required to perform picking vibration is large. During the process of positioning and clamping the camellia trunk by the picking manipulator, valve 12 will lose power, and pump 4 will be the only pump working to supply oil to the hydraulic servo system of the manipulator to realise the movement of the manipulator arm joints. After the completion of the positioning, the electromagnet on the right side of valve 7 will be energised, and motor 9 drives a bevel gear pair to rotate forward, which drives a ball screw to move to realise the closing of the gripper and clamp the camellia tree. In order to prevent the clamped camellia trunk from loosening, bidirectional hydraulic locks 8 are designed at both ends of motor 9 since the hydraulic oil flow required by the vibrating hydraulic motor 15 is relatively large during vibration picking. After clamping the camellia tree, the hydraulic lock 8 will lock the hydraulic motor 9's oil circuit. At the same time, valve 7 will be de-energised, while valve 12 will be electrified. At this time, pump 3 and 4 simultaneously supply oil to hydraulic motor 15 until the vibration ends. After the end of the vibration, the energisation of valve 12 and valve 7 will be reversed. The hydraulic motor 9 rotates in reverse, and the gripper automatically releases the camellia tree when the hydraulic lock 8 opens.

The opening and closing of the grippers are controlled by the flow direction of the oil of the hydraulic motor 9, which is realised by controlling the electrification of the solenoid valve 7. The vibration frequency of the picker is determined by the rotational speed of the hydraulic motor 15, which is designed by controlling the degree of valve opening of the electro-hydraulic proportional flow valve 12.

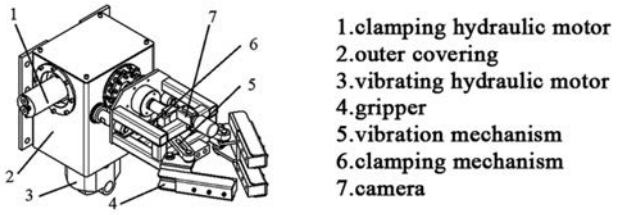

Figure 1. The structure of the vibration picking manipulator.

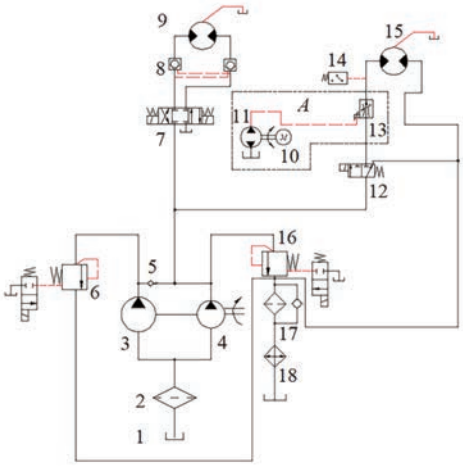

Figure 2. Hydraulic principle diagram of the vibration picking manipulator.

Establishment of mathematical system model

Establishment of the mathematical model of vibration picking actuator

The vibration picking actuator of the picking machine can be considered a crank-slider mechanism which is shown in Figure 3. The motion centre of the link l_1 coincides with the shaft of the vibrating hydraulic motor, and the link l_2 is combined with the link l_1 through a hinge, which drives slider 3 to realise linear reciprocating motion in order to create a vibration on the camellia tree.

In the steady state, the excitation force F of the vibration generated by the actuator is proportional to the angular velocity ω of the hydraulic motor. According to the circular motion law of classical physics, the relationship between the excitation frequency f and the motion angular velocity ω is obtained as:

$$f = \frac{\omega}{2\pi} \tag{1}$$

Establishment of a mathematical model of a valve-controlled vibrating hydraulic motor system

i) Mathematical model of hydraulic motor: In fluid mechanics, the fluid has the characteristics of mass conservation, so the continuity of the flow rate of the hydraulic motor can be obtained as:

$$\Delta q_m = V_{stm}\frac{d\Delta\theta_m}{dt} + K_{cm}\Delta p_m + \frac{V_m}{E_m}\frac{d\Delta p_m}{dt} \tag{2}$$

where:
q_m, hydraulic motor inlet flow;
V_{stm}, theoretical displacement of hydraulic motor;
θ_m, rotation angle of hydraulic motor output shaft;
K_{cm}, leakage coefficient of hydraulic motor;
p_m, hydraulic motor inlet pressure;
V_m, hydraulic motor inlet cavity volume;
E_m, elastic modulus of hydraulic oil.

The driving force of the hydraulic motor shaft is balanced with the inertial force, viscous resistance, and elastic force of the hydraulic motor shaft, and the reaction torque of the load on the hydraulic motor, and the following formula is summarised as:

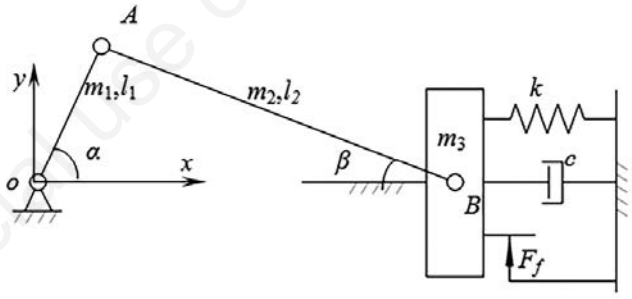

Figure 3. Schematic diagram of vibration picking actuator.

$$\frac{V_{stm}\Delta p_m}{2\pi} = J_t\frac{d^2\Delta\theta_m}{dt^2} + c_m\frac{d\Delta\theta_m}{dt} + G\Delta\theta_m + \Delta T \tag{3}$$

where:
J_t, total momentum of inertia on the hydraulic motor shaft (including loads);
c_m, viscous damping coefficients of hydraulic motors and loads;
G, torsional stiffness of loads;
T, load torque on hydraulic motor shaft.

ii) Mathematical model of actively controlled pilot-operated electro-hydraulic proportional flow valve: Component A in Figure 2 is an actively controlled pilot-operated electro-hydraulic proportional flow valve, consisting of a DC motor 10, a small quantitative hydraulic pump (motor) 11 and a pilot electro-hydraulic proportional flow valve 13. Its basic structure is shown in Figure 4. The control system drives the motor to rotate forward or reverse by controlling the input voltage signal to realise the oil suction and pressure of the hydraulic pump (motor). The hydraulic pump controls the flow of hydraulic oil entering the pilot valve, thereby realising the adjustment of the hydraulic oil flow of the main valve,

which controls the output of the vibrating hydraulic motor. The advantage of this control scheme is that it can flexibly adjust in real-time according to the output signal of the vibration sensor and maintain the stability of the flow rate of the pilot valve, which reduces the system's power loss and heat generation. In addition, it is not necessary to install a differential pressure compensator (Zhangzhou *et al*., 2022) or a flow sensor (Tsutsumi *et al*., 2007; Shang *et al*., 2019), which reduces the cost. The working principle diagram of the valve is shown in *Figure 3* in the *online Appendix*.

The following is the process of establishing the mathematical model of the actively controlled pilot-operated electro-hydraulic proportional flow valve.

According to the basic principles of physics, the DC motor drive circuit satisfies Kirchhoff's law, and the following equation is obtained in the DC motor circuit:

$$\Delta U_f = R\Delta i + L\frac{d\Delta i}{dt} + C_e\Delta\omega_0 \tag{4}$$

where:
U_f, armature voltage on the DC motor;
R, resistance of the load;
i, loop current;
L, inductance of the load;
C_e, back EMF coefficient;
ω_0, angular velocity of the motor.

According to Newton's law of motion, the output torque of the output shaft of the DC motor is balanced with the inertia moment and viscous resistance on it, so there is the following formula:

$$\Delta M = C_M\Delta i = J\frac{d\Delta\omega_0}{dt} + B\Delta\omega_0 \tag{5}$$

where:
M, motor torque;
C_M, rotational coefficient;
J, moment of inertia of motor and load;
B, viscous damping coefficient on the motor.

The flow of the pilot valve is determined by the flow of the hydraulic pump (motor), so there is:

$$q_b = nq_p = \frac{\omega_0}{2\pi}q_p \tag{6}$$

where:
q_b, pilot valve flow;
n, rev of DC motor;
q_p, pump (motor) flow.

According to Bernoulli's equation in fluid mechanics, the flow formula for the main valve port is:

$$q_M = C_{dM}W_M x\sqrt{\frac{2}{\rho}(p_A - p_B)} \tag{7}$$

The formula for the gain of the main valve opening area is:

$$W_M = \pi d_m \sin\alpha\left(1 - \frac{x}{2d}\sin 2\alpha\right)$$

The main spool displacement equation is:

$$x = \frac{q_b}{C_{dc}W_c}\sqrt{\frac{\rho}{p_A - p_B}} - x_i \tag{8}$$

The total flow of the entire hydraulic valve is the sum of the flow of the main valve port and the flow of the pilot valve, so there is the following formula:

$$q = q_M + q_b \tag{9}$$

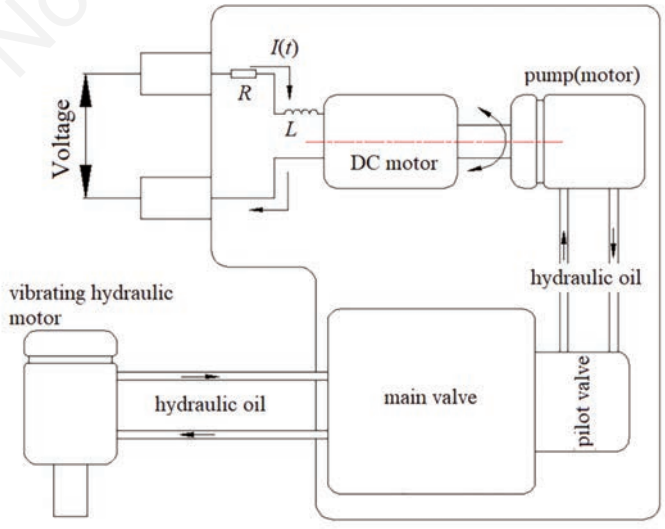

Figure 4. Actively controlled pilot-operated electro-hydraulic proportional flow valve.

Substitute Eqs. (7) and (8) into Eq. (9) to get:

$$q = \left(1 + \frac{\sqrt{2}W_m}{W_c}\right) q_b - C_{dm} W_m x_i \sqrt{\frac{2(p_A - p_B)}{\rho}} \quad (10)$$

where:
q_M, main valve port flow;
C_{dM}, main valve flow coefficient;
q_p, pump (motor) flow;
W_M, main valve opening area gain;
x, displacement of the main spool;
ρ, density of hydraulic oil;
p_A, inlet pressure;
p_B, outlet pressure;
d_m, diameter of the main valve port;
α, valve opening angle;
d, diameter of the main valve spool;
C_{dc}, flow coefficient of feedback throttling slot;
W_c, gain of the opening area of feedback throttling slot;
x_i, the pre-opening amount of feedback throttle slot.

Since the vibration frequency of the vibrating hydraulic motor is constant within a certain range, the required working flow of the oil is constant within a certain range. According to Tsutsumi *et al.* (2007), the flow equations for the pilot and main valves can be linearised around this operating point as:

$$\Delta q_b = \frac{q_p}{2\pi} \Delta\omega_0 = k_w \Delta\omega_0 \quad (12)$$

where:
k_w , flow-angular velocity coefficient of the pilot valve;

$k_{xb} = 1 + \sqrt{2} W_m / W_c$, flow coefficient of the pilot valve;

k_{qF}, flow gain of the main valve;
k_m, flow-pressure coefficient of the main valve.

iii) Derivation of state space equation of valve-controlled vibration hydraulic motor system:

A total of 5 variables, which are current increment Δi, motor angular velocity increment $\Delta\omega_0$, hydraulic motor angular displacement increment $\Delta\theta_m$, hydraulic motor shaft angular velocity increment $d\Delta\theta_m/dt$, and hydraulic motor inlet pressure p_m, are selected as state variables in the above system. In addition, choose voltage increment ΔU_f, load torque increment ΔT, and pre-opening increment of feedback throttle slot Δx_i as input variables. The following state space equations are derived by simplifying the above Eqs. (2)-(5), (11), and (12).

$$\begin{cases} \dot{x}_1 = -\frac{R}{L} x_1 - \frac{C_e}{L} x_2 + \frac{1}{L} u_1 \\ \dot{x}_2 = \frac{C_M}{J} x_1 - \frac{B}{J} x_2 \\ \dot{x}_3 = x_4 \\ \dot{x}_4 = -\frac{G}{J_t} x_3 - \frac{c_M}{J_t} x_4 + \frac{V_{stm}}{2\pi J_t} x_5 - \frac{1}{J_t} u_2 \\ \dot{x}_5 = \frac{k_{xb} k_w E_m}{V_m} x_2 - \frac{V_{stm} E_m}{V_m} x_4 + \frac{(k_m - K_{cm}) E_m}{V_m} x_5 - \frac{k_{qF} E_m}{V_m} u_3 \end{cases} \quad (10)$$

where:

The input variable matrix is:

$$u = \begin{bmatrix} u_1 & u_1 & u_1 \end{bmatrix}^T = \begin{bmatrix} \Delta U_f & \Delta T & \Delta x_i \end{bmatrix}^T$$

The state variable matrix is:

$$x = \begin{bmatrix} x_1 & x_2 & x_3 & x_4 & x_5 \end{bmatrix}^T = \begin{bmatrix} \Delta i & \Delta\omega_0 & \Delta\theta & \frac{d\Delta\theta}{dt} & \Delta p_m \end{bmatrix}^T$$

The output equation of the system is:

$$y = f = \frac{1}{2\pi} x_4$$

The above state equation and output equation can be written in matrix form:

$$\begin{cases} \dot{x} = Ax + Bu \\ y = Cx \end{cases}$$

where:

$$A = \begin{bmatrix} -\frac{R}{L} & -\frac{C_e}{L} & 0 & 0 & 0 \\ \frac{C_M}{J} & -\frac{B}{J} & 0 & 0 & 0 \\ 0 & 0 & 0 & 1 & 0 \\ 0 & 0 & -\frac{G}{J_t} & -\frac{c_m}{J_t} & \frac{V_{stm}}{2\pi J_t} \\ 0 & \frac{k_{xb} k_w E_m}{V_m} & 0 & -\frac{V_{stm} E_m}{V_m} & \frac{(k_m - K_{cm}) E_m}{V_m} \end{bmatrix}$$

$$B = \begin{bmatrix} \frac{1}{L} & 0 & 0 \\ 0 & 0 & 0 \\ 0 & 0 & 0 \\ 0 & -\frac{1}{J_t} & 0 \\ 0 & 0 & -\frac{k_{qF} E_m}{V_m} \end{bmatrix}$$

$$C = \begin{bmatrix} 0 & 0 & 0 & \frac{1}{2\pi} & 0 \end{bmatrix}$$

Design of control system

Design of PID controller

The control law of incremental digital PID is as follows:

$$\Delta u(k) = u(k) - u(k-1)$$
$$= K_p \left[e(k) - e(k-1)\right] + K_I e(k) + K_D \left[e(k) - 2e(k-1) + e(k-2)\right]$$

In the formula: $u(k)$ and $u(k–1)$ are the kth and $k–1$th output values of the controller; K_p is the proportional coefficient; K_I is the

integral coefficient; K_D is the differential coefficient; $e(k)$, $e(k–1)$, and $e(k–2)$ are the kth, $k–1$th, and $k–2$th input error values.

It is difficult to achieve the optimal control effect when the control system of the vibration hydraulic motor adopts a PID controller to adjust the three parameters of proportional, integral, and differential. Therefore, the fuzzy neural network is used to adjust these three parameters in PID adaptively. The input and output function relationship of the fuzzy neural network is shown in the following formula (13), and the control flow chart of the fuzzy neural network PID controller is presented in Figure 5.

$$\begin{cases} K_P = f_1(e, \dot{e}) \\ K_I = f_2(e, \dot{e}) \\ K_D = f_3(e, \dot{e}) \end{cases} \quad (13)$$

Design of fuzzy neural network

According to the above, this paper needs to design a fuzzy neural network to adjust the three parameters of the PID system, and the FWNN can realise the refined control of the frequency, so this paper chooses the FWNN as the fuzzy neural network for the PID control. The FWNN designed in this paper is divided into 6 layers: the input layer, fuzzification layer, fuzzy inference layer, wavelet layer, wavelet product layer, and output layer. Its structure is listed in Figure 6.

Input layer. The input layer uses two neuron nodes, representing the control system's deviation e and the deviation change rate *de/dt*. Its input activation function is $f_1(x_i)=x_i$.

Fuzzification layer. The role of this layer is to fuzzify the two inputs. The fuzzy subset of deviation e and deviation change rate *de/dt* is set as {NB, NM, NS, ZO, PS, PM, PB}, namely {negative big, negative medium, negative small, zero, positive small, positive medium, positive big}, a total of 7 neuron nodes. The designed fuzzy neural network PID controller adopts incremental PID control. The fuzzy neural network is used to locally fine-tune the three parameters of K_p, K_i, and K_d to determine the basic range of PID controller parameters. Therefore, the range of the fuzzy set can be set to be very small. In this paper, the value range of the fuzzy set is set to [–6, 6] according to Xu *et al.* (2022). Its input can be expressed as:

$$r_{ij} = x_i + \mu_{ijn-1}\alpha_{ij} \quad (9)$$

where:
n, number of iterations;
α_{ij}, the weight of recursive feedback connection;
μ_{ijn-1} , Gaussian membership function.

The output signal of the second layer is:

$$f_2(i,j) = \exp\left(-\frac{(r_i - c_{ij})^2}{(b_j)^2}\right)$$

In the formula: i=1,2; j=1,2,...,n; c_{ij} and b_j represent the centre value and width value of the membership function, respectively.

i) Fuzzy inference layer: The main function of this layer is to perform fuzzy reasoning according to the set fuzzy rule table to determine the changing trend of PID parameters. In addition, this layer completes the matching of fuzzy rules through the connection with the fuzzification layer and performs fuzzy operations between nodes. The calculation formula used in this layer is:

$$f_3(j) = \prod_{j=1}^{N} \mu_{ij}(f_2(i,j))$$

where:

$N = \prod_{i=1}^{n} n_i$, sum of neurons.

ii) Wavelet layer: The primary purpose of the wavelet layer is to perform frequency segmentation on the third layer. Therefore, each input signal $f_3(j)$ from layer 3 is passed through the activation function of the wavelet node. The activation function is:

$$f_4(j) = \left(1 - \frac{\|f_3(j) - t_j\|^2}{d_j^2}\right)\exp\left(-\frac{\|f_3(j) - t_j\|^2}{2d_j^2}\right)$$

where:
d_j, scaling parameters of wavelet nodes;
t_j, translation parameters for wavelet nodes;
w_j, the weight of the jth node of the neural network.

iii) Wavelet product layer: This layer is similar to the third layer of fuzzy inference, which completes matching fuzzy rules through the connection with the wavelet layer and performs fuzzy operations between nodes. The main purpose of designing this layer is to perform fuzzy reasoning on the results after waveletization to determine a more precise adjustment range of PID parameters.

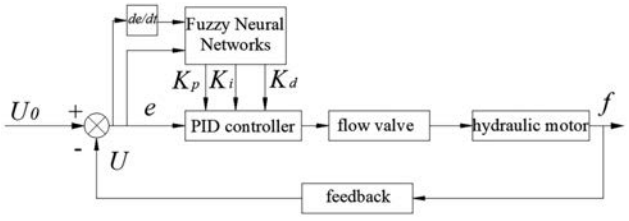

Figure 5. Control flow chart of the fuzzy neural network PID controller.

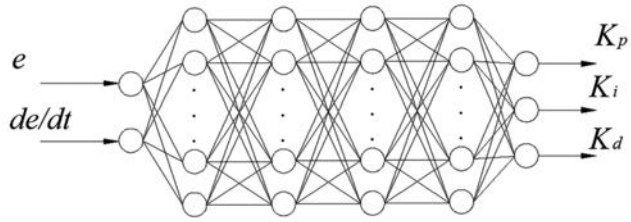

Figure 6. Structure of the fuzzy wavelet neural network.

The calculation formula used in this layer is:

$$f_5(j) = \prod_{j=1}^{N} (f_4(j))$$

where:

$N = \prod_{i=1}^{n} n_i$, sum of neurons.

iv) Output layer: The role of this layer is to output the three control parameters of the PID controller. Its calculation formula is:

$$f_6(i) = w \bullet f_5 = \sum_{j=1}^{N} w(i,j) \bullet f_5(j)$$

which is:

$$K_P = \sum_{j=1}^{N} w(1,j) \bullet f_5(j)$$

$$K_i = \sum_{j=1}^{N} w(2,j) \bullet f_5(j)$$

$$K_d = \sum_{j=1}^{N} w(3,j) \bullet f_5(j)$$

where:

Among them, w is the connection weight matrix between the fuzzy inference and output layers.

The gradient descent method is used to adjust the neural network parameters to determine the network weights. The performance indicators of the neural network are selected as follows:

$$E = \frac{1}{2}[e(k)]^2$$

The update equations of the fourth layer wavelet scaling d_j and translation parameters t_j are:

$$d_{ij}(k) = d_{ij}(k-1) + \Delta d_{ij}(k) + \alpha\left[d_{ij}(k-1) - d_{ij}(k-2)\right]$$

$$t_j(k) = t_j(k-1) + \Delta t_j(k) + \alpha\left[t_j(k-1) - t_j(k-2)\right]$$

$$\Delta d_{ij} = -\eta \frac{\partial E}{d_{ij}}$$

$$\Delta t_j = -\eta \frac{\partial E}{t_j}$$

The weight update equation of the output layer of the sixth layer is:

$$w(k) = w(k-1) + \Delta w(k) + \alpha\left[w(k-1) - w(k-2)\right]$$

$$\Delta\omega(k) = -\eta \frac{\partial E}{\partial \omega}$$

where:
η, learning rate;
α, momentum factor.

Field test and simulation analysis

Analysis of the result of the simulation of the control system with MATLAB/Simulink

A simulation experiment was carried out in MATLAB/Simulink to verify the effect of the FWNN PID controller designed in this paper to provide a theoretical basis for the design of the picker control system. The built FWNN PID controller simulation module is shown in Figure 7.

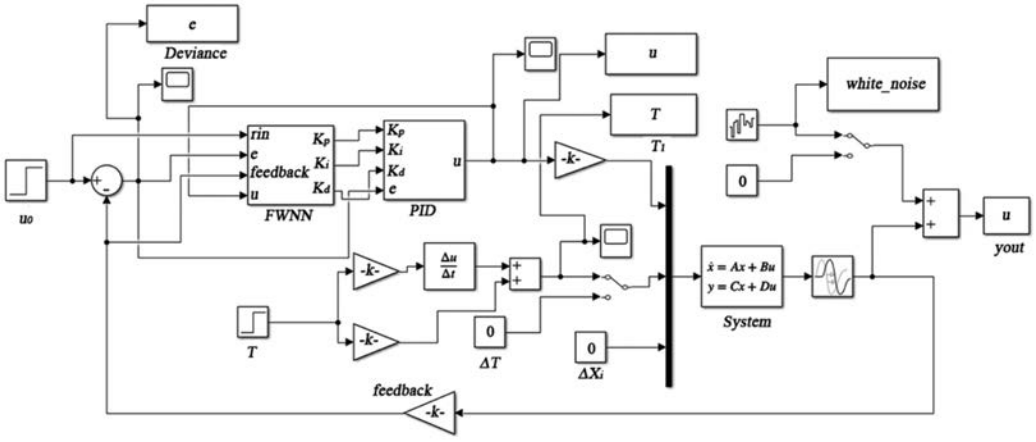

Figure 7. Fuzzy wavelet neural network PID controller designed in Simulink.

The simulation running environment was MATLAB R2018a with Windows 10 64-bit operating system, while the computer CPU was Intel Core i5-9400F, whose main frequency was 2.9 GHz, and the memory was 16GB. The parameters used in the simulation are shown in additional documents.

In the simulation experiment, the step signal was selected as the simulation input, and the simulation time was set to 10 s. The general PID controller, fuzzy PID controller, and a fuzzy RBF neural network PID controller (FRBFNN PID controller) were used in the simulation to compare to verify the effect of the control strategy selected in this paper.

Simulation condition 1: no-load condition

In the case of no-load, this paper set the step signal input of 12V at 0s. As a result, the step response curve obtained by the simulation is obtained as shown in Figure 8.

It can be seen from Figure 8 that the general PID controller did not have the self-tuning capability. When taking the allowable error △=2%, it took 4.82 s to reach a steady state, and the maximum overshoot was 17.28%. The FPID controller had a specific self-tuning capability, it spent 3.74 s reaching a steady state, and the maximum overshoot was 9.23%. The FRBFNN PID controller had a better self-tuning capability. It took 3.18 s to achieve a steady state, and the maximum overshoot was 4.58%. The entire system only oscillated slightly. The parameter self-tuning of the FWNN controller was the best among these four controllers. It spent 2.77 s reaching a steady state, and the maximum overshoot was 2.46%. The system did not oscillate substantially with this kind of controller. The smaller the system overshoot is, the better the camellia flower drop rate can be controlled, and the faster the time response, the higher the picking efficiency. It can be seen from the analysis of the above results that the fuzzy neural network PID controller has the above advantages, and its time response performance is good.

Simulation condition 2:5 s load after startup

In this paper, a step input voltage of 12 V was still input to the four systems at 0 s, and an external load of 45.5 Nm was applied to the system after 5 s of no-load operation. The simulation results are presented in Figure 9.

After the 45.5 Nm load was connected, the system instantly generated a load shock of 53.5 Nm. The system using a general PID controller succumbed to this effect, causing a frequency fluctuation with a duration of 2.78 s and a frequency drop of 2.46 Hz. The system using an FPID controller produced a frequency fluctuation of up to 1.15 s and a frequency drop of 1.03 Hz. This impact brought the system using the FRBFNNPID controller on a frequency fluctuation of up to 0.54 s and a frequency drop of 0.222 Hz, while the system with the FWNNPID controller generated a frequency fluctuation of 0.48 s and a speed drop of 0.194 Hz under this impact. It can be seen that the fuzzy neural network PID controller has the characteristics of good load-carrying robustness.

Simulation condition 3: start with load

At 0 s, the control system carried a 45.5 Nm external load while inputting a 12 V step input voltage to the four systems. The simulation results are shown in Figure 10.

It can be seen from the simulation results in Figure 10A that when the vibration was directly started with load at 0 s, the controlled valve-controlled vibration hydraulic motor system with PID controller could not be able to start immediately but could respond to drive the camellia tree to vibrate after 1.73 s. The system using the FPID controller would not start immediately, but only after 1.01 s would respond to drive the tree to vibrate. The system controlled by the FRBFNN PID controller could quickly respond to generate the vibration after 0.62 s. The system controlled by the FWNN PID controller responded after 0.45 s by vibrating the tree.

It can be seen by comparing the simulation results in Figure 10A-C that in the case of starting with load, the error value of the system controlled by the FWNN PID controller reaches the maximum at 0.26 s, and the frequency drop value of the vibration hydraulic motor reaches the maximum at this time. At this time, the fuzzy neural network quickly adjusts and changes the values of K_p, K_i, and K_d, thereby rapidly increasing the PWM duty cycle of the DC motor drive to change the output flow of the electro-hydraulic proportional flow valve and adjust the rotational speed of the vibrating hydraulic motor, so that the error value of the system decreases rapidly. At 1.84 s, the fuzzy neural network changes the

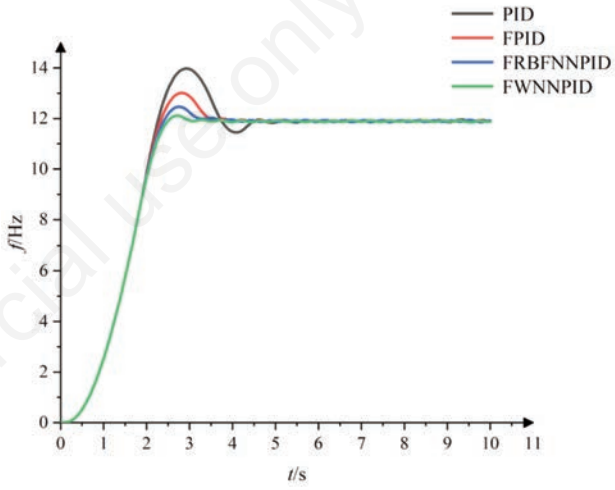

Figure 8. Simulation of no-load condition. FRBFNN PID controller, fuzzy RBF neural network PID controller; FWNN PID controller, fuzzy wavelet neural network PID controller.

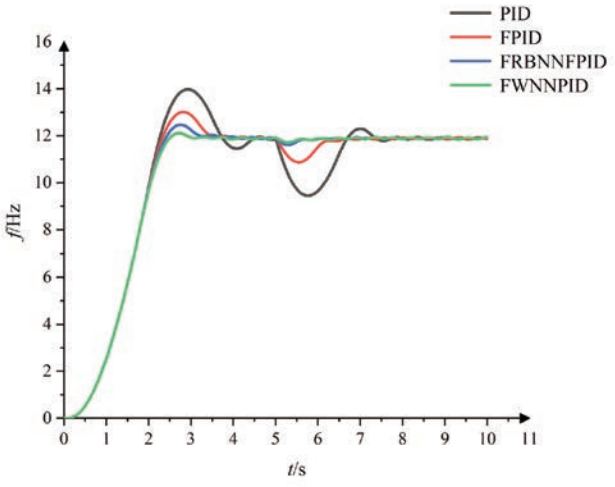

Figure 9. Simulation of load condition after 5 s. FRBFNN PID controller, fuzzy RBF neural network PID controller; FWNN PID controller, fuzzy wavelet neural network PID controller

values of K_p, K_i, and K_d to slightly reduce the PWM duty cycle of the DC motor to reduce the opening of the valve, thereby reducing the growth rate of the rotational speed of the vibrating hydraulic motor and decrease the error rate of the system. At 2.78 s, the overshoot of the system reaches the maximum value. The fuzzy neural network adjusts the parameter K_p, K_i, and K_d to reduce the PWM duty cycle of the DC motor. At this time, the valve port of the pilot valve of the electro-hydraulic proportional flow valve is close to closing, and the main valve's flow decreases, reducing the rotational speed of the hydraulic motor. The error value of the whole system gradually changes from a negative value to a positive value. At 3.29 s, the system is basically in a stable state, and the error value of the system is, on the whole, stable within the allowable range. At this time, the driver of the DC motor stabilises the output voltage. The controller no longer changes the duty cycle of the PWM. The FRBFNN PID controller has a slower response speed, longer adjustment time, and a larger rotational speed difference of the vibration hydraulic motor than the FWNN PID controller. The delay time of on-load start-up of the system using the FWNN PID controller is almost negligible considering the actual outdoor working conditions in woodland. The camellia fruit picking machine requires to complete the picking of a tree within two minutes. The system adjustment time in 3.29 s is almost negligible in comparison, and the shorter oscillation time and overshoot are also beneficial to ensure that the drop rate of camellia flowers is controlled within a certain range.

A white noise signal with intensity from –3 Hz to 3 Hz was applied to the end of the control system's output to simulate the influence of external disturbances on the control system under the above simulation condition. The simulation result is shown in Figure 10D. It can be seen from the above simulation results that when the FWNNPID controller is subjected to the same degree of external disturbance, its fluctuation amplitude is smaller than that of the FRBFNNPID controller, and its vibration frequency can basically keep floating around 12 Hz, of which upper and lower frequency fluctuation does not exceed ±0.5 Hz. This means that the fuzzy neural network PID control system can ensure that the vibration frequency of the system is controlled within a specific range when subjected to external disturbances, thereby avoiding the fall of camellia flowers. Therefore, the fuzzy neural network PID controller can directly meet the requirements of immediately starting vibration picking after clamping the camellia tree, greatly improving the picking efficiency. At the same time, its time response characteristics and robustness are better compared with PID and FPID controllers.

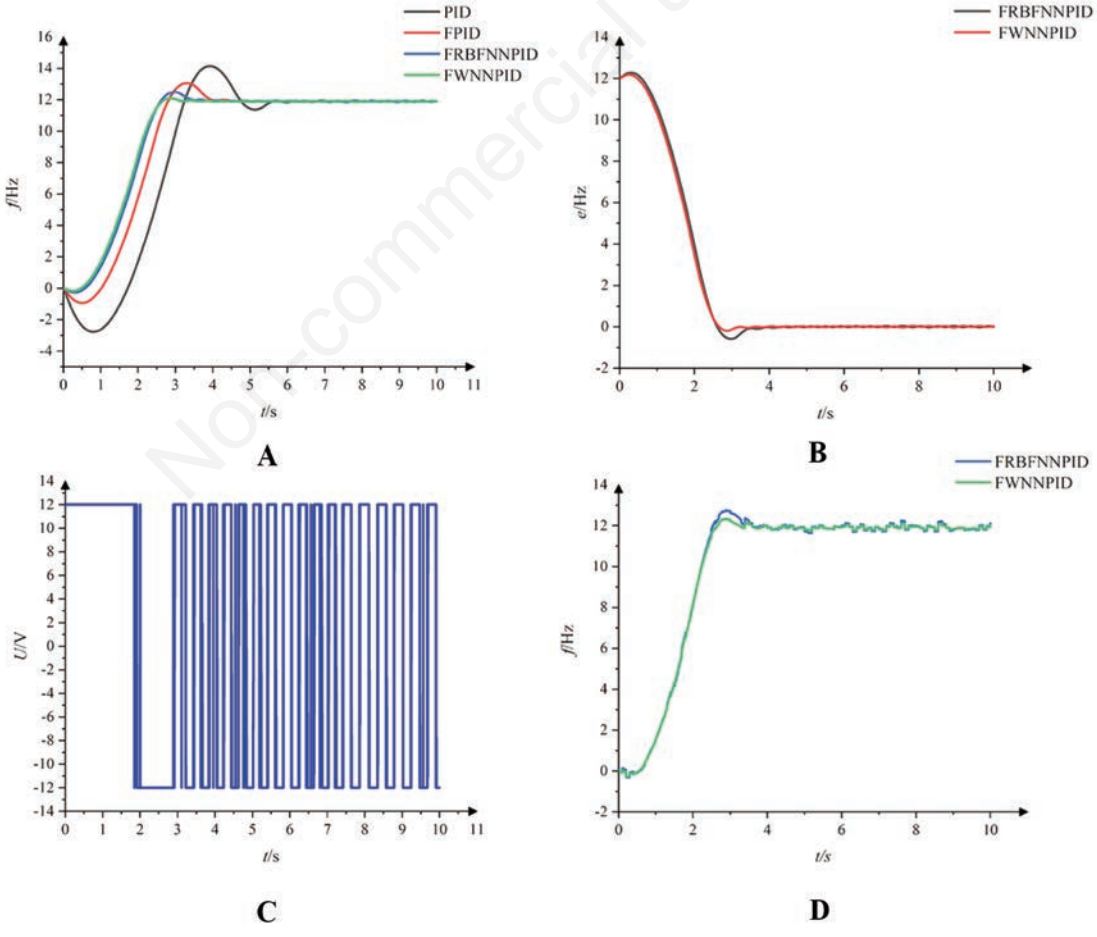

Figure 10. A-D) Simulation of start with load condition. FRBFNN PID controller, fuzzy RBF neural network PID controller; FWNN PID controller, fuzzy wavelet neural network PID controller.

Analysis of the result of the field test

The above simulation results theoretically prove that the fuzzy neural network PID controller has a better control effect than other controllers. Therefore, the camellia fruit picking manipulator controller shown in Figure 1 was designed according to the above control principle. A field test was carried out to verify whether the designed controller is adaptable to camellia picking. Our research team conducted a camellia fruit field test on October 18, 2021, at the experimental base of Xuefengshan Camellia Society in Wangcheng District, Changsha City, Hunan Province. The test time was 9:30 a.m., the weather was cloudy, the temperature was 15°C, and the air humidity was 86%. The designed test prototype is shown in Figure 11. The prototype adopted the PID controller, fuzzy RBF neural network PID controller, and the fuzzy wavelet neural network PID controller, to carry out the picking test. The picking effect is shown in Figure 11.

The control system of the prototype consists of a single-board computer, a driver, motion controllers, and sensors. The upper computer adopts the single-board computer EasyDL-JetsonNano, mainly used for receiving sensor signals, image processing, and motion position calculation, while the lower computer adopts the single-chip STM32F405RGT6 as the controller of the actuator. A KSI84 Ax vibration sensor is installed at the end of the shaft end of the manipulator's vibrating hydraulic motor to measure the vibrating hydraulic motor's output amplitude and frequency.

The prototype of the camellia fruit picking machine first determined a camellia tree to be picked through its vision system (monocular camera with FUJINON HF16SA-1 and binocular CMOS camera) and transmitted the data of the tree to the Jetson Nano. The Jetson Nano automatically planned the picking manipulator movement trajectory according to the transmitted data and calculated the joint angles driven by the hydraulic cylinders and hydraulic motors required for each movement. Then it transmitted the signal to the lower computer to drive the picking manipulator to move and hold the target camellia tree. After the sensor transmitted the clamping signal for 5 s, the lower computer controlled

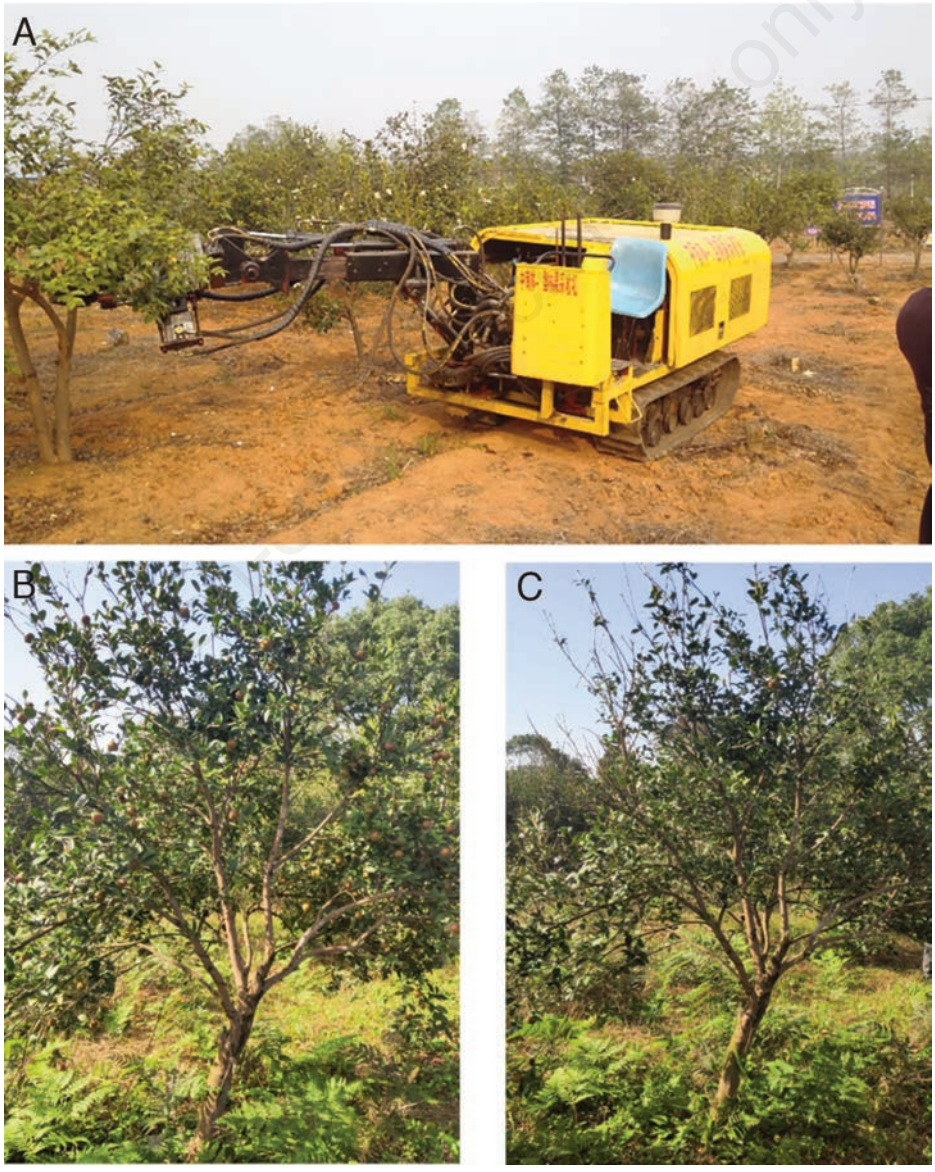

Figure 11. A-C) Field picking test.

Table 1. Picking test results of PID controller.

Controller	Average picking time (s)	Average rate of dropping flowers (%)	Average rate of dropping fruits (%)
PID controller	124.8	10.0	83.9
FRBFNN PID controller	97.9	6.8	90.9
FWNN PID controller	92.1	4.8	92.3

FRBFNN PID controller, fuzzy RBF neural network PID controller; FWNN PID controller, fuzzy wavelet neural network PID controller.

the input voltage of the DC motor to control the opening of the active pilot electro-hydraulic proportional flow valve in order to realize the control of the frequency of the vibrating hydraulic motor. After picking, the gripper of the picking actuator opened to a given angle, and the picking manipulator moved back to the set initial coordinate position.

The results of the picking test using the PID controller, fuzzy RBF neural network PID controller, and fuzzy wavelet neural network PID controller are shown in Table 1.

Within the first 5 s after the start of vibration picking, the leaves and camellia flowers on the camellia trees fell off the bench, visible by eyes under the prototype controlled by the FRBFNN PID controller. After the first 5 s, the camellia fruit basically fell stably from the camellia trees, and the camellia flowers did not fall, visible to eyes. However, in the first 5 s after picking, the leaves on the camellia trees picked by the prototype controlled by the FWNN PID controller fell off the bench visible to eyes, while the camellia flowers did not fall from the trees significantly, at least from what it was visible to the naked eye. After 5 s, camellia fruit basically fell stably from the camellia tree.

It can be seen from the above test results that adjusting the excitation frequency of the picker to 12 Hz can maintain a low flower drop rate and a relatively high fruit drop rate. The machine with the fuzzy neural network PID controller can significantly shorten the picking time, reduce the falling rate of camellia flowers, and improve the picking efficiency compared with the PID controller. The average working time of the picking machine controlled by the FRBFNN PID controller is longer than that controlled by the FWNN PID controller. Using FWNN PID controller can significantly reduce the drop rate of camellia flowers with a high picking efficiency of fruits. The above experimental results show that the FWNN PID controller can further meet the needs of the picking operation of camellia fruits.

Conclusions

In order to solve the problem that the camellia fruit picking machine needs to ensure that the vibration frequency is controlled within a specific range, this paper deduced the state space equation of the valve-controlled hydraulic system of the vibration part of the machine. On this basis, an FWNN PID controller was designed, and the simulation verification and experimental verification analysis were carried out under no-load, 5 s loaded, and start-up loaded. The simulation results show that the FWNN PID controller method has a faster response and better robustness than the general PID controller, fuzzy PID controller, and FRBFNN PID controller in the constant speed control of the vibrating hydraulic motor. Moreover, the field test results show that the FWNN PID controller can effectively control the falling rate to a lower value while ensuring the picking efficiency and can better meet the control requirements of the vibration frequency of the vibrating hydraulic motor.

References

Ayas M.S., Altas I.H. 2018. Designing and implementing a plug-in type repetitive controller for a redundantly actuated ankle rehabilitation robot. Proceedings of the Institution of Mechanical Engineers, Part I. J. Syst. Control Engine. 232:592-607.

Ayten K.K. 2019. A. Implementation a fractional-order adaptive model-based PID-type sliding mode speed control for wheeled mobile robot. Proceedings of the Institution of Mechanical Engineers, Part I. J. Syst. Control Engine. 233:1067-84.

Gao Z.C., Li L.J., Li X. 2013. Development and experiment of the picking actuator of the comb-type camellia fruit picking machine. Trans. Chinese Soc. Agric. Engine. 29:19-25.

Gao Z.C., Li L.J., Wang P.H., Zhu Q., Luo Y.K. 2016. The design and analysis of Camellia fruit picking 'robots' picking monomers. J. Central South Univ. Forestry Technol. 36:114-8.

Gao Z.C., Zhao K.J., Li L.J., Pang G.Y., Wang X.C. 2019. Design and test of suspension vibrating camellia picking executing mechanism. Trans. Chinese Soc. Agric. Engine. 35:9-17.

Gong C., Yang S.Q. 2019. Research of oil pump control based on fuzzy neural network PID algorithm. Int. J. Adv. Netw. Monit. Control. 3:63-8.

Guo H.L., Li K.W. 2012. Research on control system for sluice gate flow based on fuzzy neural network PID. Appl. Mechan. Mater. 1945:1779-82.

Han S.Y., Dong J.F., Zhou J., Chen Y.H. 2022. Adaptive fuzzy PID control strategy for vehicle active suspension based on road evaluation. Electronics. 11:921.

Huang D., Rao H.H. 2019. Research present situation of mechanized picking equipment for camellia in China. Forest. Machine. Woodwork. Equip. 47:11-3.

Karaboga D., Akay B. 2010. Proportional-integral-derivative controller design by using artificial bee colony, harmony search, and the bees algorithms. Proceedings of the Institution of Mechanical Engineers, Part I. J. Syst. Control Engine. 224:869-83.

Kong L., Yuan J. 2020. New relaxed stabilization conditions for discrete-time Takagi-Sugeno fuzzy control systems. Asian J. Control. 22:1604-16.

Lin B., Su X.Y., Li X.H. 2019. Fuzzy sliding mode control for active suspension system with proportional differential sliding mode observer. Asian J. Control. 21:264-76.

Meng F.H., Zhao S.S., Yu Z.P., Wang N., Gao F. 2016. Single neural element PID control based on AMESim and Simulink co-simulation for speed governing system of value-controlled motor. Chinese Hydr. Pneumat. 7:83-8.

Shang X., Zhou H., Yang H.Y. 2019. Research status of active control of hydraulic fluid pulsation. J. Mechan. Engine. 55:216-26.

Tsutsumi T., Tanino M., Yamakita J. 2007. Hydraulic valve control method of tractor implements for agricultural applications. J. Japan. Soc. Agric. Machin. 69:83-90.

Tufan D., Serhat C.M. 2022. Design and robustness analysis of fuzzy PID controller for automatic voltage regulator system

using genetic algorithm. Trans. Inst. Measure. Control. 44: 1862-73.
Wang C.Y., Li L.J. 2019. Hand-eye calibration algorithm for robot based on quaternion. Transd. Microsyst. Technol. 38:133-5.
Wang P.H., Li L.J., Gao Z.C., Min S.H., Xiao J. 2015. The design and analysis of oscillating fruit picking head. J. Northw. Forest. Univ. 30:288-91.
Wang W.J., Chen C.G., Cheng J. 2007. Active role of tea oil in medicine and health care. Food Nutr. China. 9:48-51.
Wang Z., Huang Y.S. 2019. Robust decentralized adaptive fuzzy control of large-scale nonaffine nonlinear systems with strong interconnection and application to automated highway systems. Asian J. Control. 21:2387-94.
Wu Q.C., Zhang Y.M., Chen Y. 2022. Design, control, and experimental verification of a soft knee exoskeleton for rehabilitation during walking. Proceedings of the Institution of Mechanical Engineers, Part I. J. Syst. Control Engine. 236:138-52.
Xu J.J., Xiao L., Lin M.Q., Tan X.J., Su J. 2022. Application of fuzzy PID position control algorithm in motion control system design of palletizing robot. Secur. Commun. Netw. 2022. [Epub ahead of print].
Xue F.F., Fan Z.M. 2022. Kinematic control of a cable-driven snake-like manipulator for deep-water based on fuzzy PID controller. Proceedings of the Institution of Mechanical Engineers, Part I. J. Syst. Control Engine. 236:989-98.
Yan Z. 2020. Research on dynamic characteristics of angular displacement servo system of valve control hydraulic motor. Chinese Hydr. Pneum. 6:43-51.
Zhang L.Y., Rao H.H., Huang D.S., Chen B., Liu M.H. 2017. Design and experiment of mechanical picking platform of camellia based on Matlab. China Southern Agric. Machin. 48:22-4.
Zhang X.Z., Li L.J. 2019. Research of image recognition of camellia oleifera fruit based on improved convolutional autoencoder. J. Forest. Engine. 4:118-24.
Zhangzhou J.Y., Chen Z.W., Dai J.C., Xu X.Q., Guo Y. 2022. Valve-cylinder integrated modeling and control strategy design for hydraulic servo vibration system. Mechan. Engine. 1:34-8.
Zhou Z.C., Chen R. 2013. Design on fuzzy neural network PID control system of diesel engine. Adv. Mater. Res. 2534:425-9.

Online supplementary material:
Part I. Introduction of camellia fruit picking background technology
Part II. Supplementary description of the mathematical model of the plant
Part III. Stability analysis of controlled system